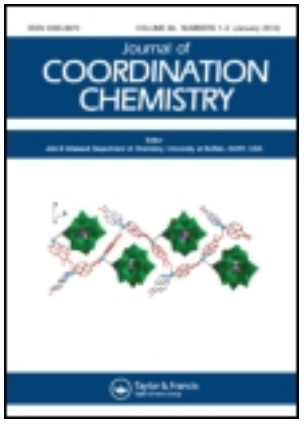

Journal of Coordination Chemistry
Publication details, including instructions for authors and subscription information:
http://www.tandfonline.com/loi/gcoo20

Experimental and computational studies of bis[bis(2-furyl)glyoximato]nickel(II)

Ayşın Zülfıkaroğlu [a], Çığdem Yüksektepe Ataol [b], Hümeyra Bati [c] & Orhan Büyükgüngör [d]

[a] Department of Chemistry, Faculty of Arts and Sciences, Amasya University, 05000 Amasya, Turkey

[b] Department of Physics, Faculty of Science, Cankiri Karatekin University, 18100-Ballica, Cankiri, Turkey

[c] Department of Chemistry, Faculty of Arts and Sciences, Ondokuz Mayis University, 55139-Kurupelit, Samsun, Turkey

[d] Department of Physics, Faculty of Arts and Sciences, Ondokuz Mayis University, 55139-Kurupelit, Samsun, Turkey

Published online: 05 Apr 2012.

To cite this article: Ayşın Zülfıkaroğlu, Çığdem Yüksektepe Ataol, Hümeyra Bati & Orhan Büyükgüngör (2012) Experimental and computational studies of bis[bis(2-furyl)glyoximato]nickel(II), Journal of Coordination Chemistry, 65:9, 1525-1538, DOI: 10.1080/00958972.2012.675432

To link to this article: http://dx.doi.org/10.1080/00958972.2012.675432

Journal of Coordination Chemistry
Vol. 65, No. 9, 10 May 2012, 1525–1538

Experimental and computational studies of bis[bis(2-furyl)glyoximato]nickel(II)

AYŞİN ZÜLFİKAROĞLU†, ÇİĞDEM YÜKSEKTEPE ATAOL*‡, HÜMEYRA BATI§ and ORHAN BÜYÜKGÜNGÖR¶

†Department of Chemistry, Faculty of Arts and Sciences, Amasya University, 05000 Amasya, Turkey
‡Department of Physics, Faculty of Science, Cankiri Karatekin University, 18100-Ballica, Cankiri, Turkey
§Department of Chemistry, Faculty of Arts and Sciences, Ondokuz Mayis University, 55139-Kurupelit, Samsun, Turkey
¶Department of Physics, Faculty of Arts and Sciences, Ondokuz Mayis University, 55139-Kurupelit, Samsun, Turkey

(*Received 28 September 2011; in final form 21 February 2012*)

Bis[bis(2-furyl)glyoximato]nickel(II) has been synthesized and characterized by infrared (IR), ^{1}H-NMR, ^{13}C-NMR, and UV-Vis spectroscopy, elemental analysis, and single-crystal X-ray diffraction. The new complex crystallizes in orthorhombic space group P_{bcn}. Mononuclear Ni^{II} complex has been obtained with 1 : 2 metal/ligand ratio. In addition to the crystal structure, the molecular geometry, vibrational frequencies, chemical shifts, molecular electrostatic potential, and frontier molecular orbital analysis of the title compound in the ground state have been calculated using the B3LYP/LANL2DZ and B3LYP/3-21 G methods. The computed vibrational frequencies are used to determine the types of molecular motions associated with each of the observed experimental bands. IR analyses show that calculated O–H stretching vibrations have lower value than experimental due to interligand O···H···O hydrogen bonds.

Keywords: *vic*-Dioxime; Ni(II) complex; Single crystal; Density functional theory; Vibrational assignment

1. Introduction

vic-Dioximes and their derivatives are an important class of ligands, forming complexes with transition metals. Since 1905, when Tschugaeff first introduced dimethylglyoxime as a reagent for nickel, numerous transition metal complexes of these ligands have been investigated [1–11]; hydrogen bridges stabilize the planar structure of *vic*-dioxime complexes. These complexes have exceptional stability and unique electronic properties [12]. Potential applications of *vic*-dioximes and their coordination compounds are useful in analytical, pigment, biological chemistry, chemical industry, medicinal chemistry, and model compounds [1]. For example, *vic*-dioximes mimic biofunctions,

*Corresponding author. Email: yuksektepe.c@karatekin.edu.tr, yuksekc@yahoo.com

ISSN 0095-8972 print/ISSN 1029-0389 online
http://dx.doi.org/10.1080/00958972.2012.675432

such as the reduction of vitamin B12. In addition, oxime metal chelates are biologically active and semiconducting [2, 13].

We have prepared a new *vic*-dioxime complex. Synthesis, characterization, and spectroscopic properties of the new *vic*-dioxime Ni(II) complex have been investigated. The complex has been identified by a combination of ^{1}H-NMR and ^{13}C-NMR spectra, FT-IR spectra, UV-Vis spectra, magnetic susceptibility measurements, and single-crystal X-ray diffraction. Molecular structure, vibrational assignments, chemical shifts, frontier molecular orbital (FMO) analysis, and molecular electrostatic potential (MEP) of bidentate transition metal complexes in the ground state have been investigated using density functional theory (DFT/B3LYP). The first aim of this study is to understand its crystal and molecular structures by X-ray analysis and quantum chemical method, comparing experimental, and theoretical results.

2. Experimental and theoretical methods

2.1. *Physical measurements*

UV-Vis spectra were recorded with a Unicam UV2-100 UV-Visible spectrometer in DMSO. Infrared (IR) spectra were recorded on a Bruker Vertex 80 V FT-IR spectrophotometer in KBr pellets. ^{1}H-NMR spectra were recorded on Bruker Avance II 400 MHz FT-NMR spectrometer utilizing deuterated DMSO as solvent. The magnetic susceptibilities were measured using a Sherwood Scientific MX1 model Gouy magnetic susceptibility balance at room temperature. pH measurements were done with a Gresiger Electronic GPHR 1400 pH meter.

2.2. *X-ray crystallography*

The data collection was performed at 293 K on a Stoe-IPDS-2 image plate detector using graphite monochromated Mo-Kα radiation ($\lambda = 0.71073$ Å). Data collection and cell refinement were performed using X-AREA [14] and X-RED32 [14]. The structure was solved by direct methods using SHELXS-97 [15] and refined by a full-matrix least-squares procedure using SHELXL-97 [15]. Molecular graphics were performed using ORTEP-3 [16]. All non-hydrogen atoms were easily found from the difference Fourier map and refined anisotropically. H4 was located in a difference Fourier map and refined isotropically (O–H = 0.867(19) Å). The other hydrogen atoms were included using a riding model and refined isotropically with C–H = 0.93 Å and $U_{iso}(H) = 1.2U_{eq}(C)$. Relevant crystal data and details of the structure determinations are given in table 1.

2.3. *Synthesis of Ni(II) complex*

A solution of $NiCl_2 \cdot 6H_2O$ (0.27 g, 1 mmol) in 10 mL ethanol was added to a solution of α-Furil dioxime (0.44 g, 2 mmol) in 20 mL ethanol. The mixture was stirred 3–4 h at 30–40°C. The pH of the solution decreased from 6–7 to 2–2.5 and then adjusted to 5–5.5 with 1% KOH solution. The turbid mixture was stirred in a water bath at 40–50°C for 1

Table 1. Crystallographic data of **1**.

Empirical formula	$C_{20}H_{14}N_4O_8Ni$
Formula weight (g mol^{-1})	497.04
Temperature (K)	296
Wavelength (Å)	0.71073
Crystal system	Orthorhombic
Space group	P_{bcn}
Unit cell dimensions (Å)	
a	19.6941(11)
b	14.1479(10)
c	6.9024(4)
Volume (Å^3), *Z*	1923.23(20), 4
Calculated density (Mg m^{-3})	1.717
Crystal size (mm^3)	$0.680 \times 0.340 \times 0.150$
θ range for data collection (°)	1.44–27.28
Limiting indices	$-24 \le h \le 22$; $-15 \le k \le 17$; $-8 \le l \le 7$
Measured reflections	6763
Independent reflections	2047
Observed reflections [$I > 2\sigma$]	1643
Max. and min. transmission	0.620 and 0.852
Goodness-of-fit on F^2	1.089
Final *R* indices [$I > 2\sigma(I)$]	$R_1 = 0.053$, $wR_2 = 0.119$
R indices (all data)	$R_1 = 0.064$, $wR_2 = 0.125$
Largest difference peak and hole (e Å^{-3})	−1.185 and 1.023
$\Delta\rho_{rms}$ (e Å^{-3})	0.18

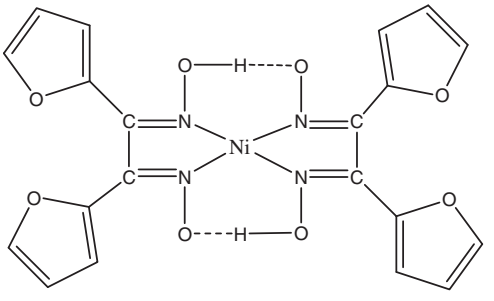

Scheme 1. The chemical diagram of bis[bis(2-furyl)glyoximato]nickel(II).

hour to completely precipitate the complex. The precipitated complex was filtered off, washed with ethanol, dried and crystallized from tetrahydrofuran–chloroform–ethyl acetate (1 : 1 : 1) (Yield: 72%) (scheme 1).

2.4. *Theoretical methods*

Starting geometry of **1** was taken from the X-ray refinement data. The molecular structure of **1** ($C_{20}H_{14}N_4O_8Ni$) in the ground state (*in vacuo*) was optimized by DFT methods to include correlation corrections with the 3-21 G and LANL2DZ basis sets.

In DFT calculations, hybrid functionals are also used, including Becke's three-parameter functional (B3) [17], which defines the exchange functional as linear combination of Hartree–Fock, local, and gradient-corrected exchange terms. The B3 hybrid functional was used in combination with the correlation functionals of Lee *et al*. [18].

Then vibrational frequencies for optimized molecular structures were calculated. The geometry with that of tetramethylsilane (TMS) is fully optimized. ^{1}H- and ^{13}C-NMR chemical shifts are calculated within the GIAO approach [19, 20] applying the B3LYP method with 3-21 G and LANL2DZ basis sets. ^{1}H and ^{13}C isotropic magnetic shielding (IMS) of any X carbon, to the average ^{13}C IMS of TMS: $CSx = IMS_{TMS}–IMS_x$. The lowest unoccupied molecular orbital (LUMO), highest occupied molecular orbital (HOMO) energy differences for these species were calculated with this method. All the calculations were performed using the Gaussview molecular visualization program [21] and Gaussian 03 on a personal computer [22].

3. Results and discussion

3.1. *Crystal structure of Ni(II) complex*

The X-ray structure of bis[bis(2-furyl)glyoximato]nickel(II) [$Ni(LH)_2$] was determined to confirm the assigned structure and establish conformation of the molecule. ORTEP drawing of the structure with atomic numbering is shown in figure 1(a) and selected geometric parameters are given in table 2. The mononuclear Ni(II) complex crystallizes in the orthorhombic space group P_{bcn} with unit cell parameters $a = 19.6941(11)$ Å, $b = 14.1479(10)$ Å, $c = 6.9024(4)$ Å, $\alpha = \beta = \gamma = 90^\circ$ with four molecules in the unit cell. The Ni, which lies on a site of -1 symmetry, is coordinated by four oxime nitrogen atoms arising from two bidentate molecules. The local coordination of NiN_4 is distorted square planar (D_{2h} symmetry). The ligand : metal ratio was 2 : 1 for mononuclear Ni(II) complex. The coordination plane around Ni and the plane of the chelating ligand coincide within experimental error. The dihedral angles between furan rings A (O1–C4) and B (O3–C10) with five-membered chelate ring C (NiN_2C_2) are $A/C = 18.53(12)^\circ$, $B/C = 38.85(10)^\circ$, and $A/B = 45.70(13)^\circ$. The Ni−N distances are different from the distances found in related complexes [6, 7], possibly attributed to the different groups attached to oxime C5 and C6. Oxime groups possess stronger hydrogen-bonding capabilities than alcohols, phenols, and carboxylic acids [23]. The hydrogen-bond systems in the crystals of oximes correlate hydrogen-bonding and N−O bond lengths [24]. The configurational and/or conformational isomers of glyoxime derivatives (dioximes) have also been analyzed [25]. The different N−O bond lengths reflect chemically distinct oxygen atoms. Comparison of the bond lengths of oxime with those of the free ligand [26] reveals that, upon complex formation, the N2−O4, N1−O2, and C5−C6 distances are shortened by 0.084, 0.066, and 0.013 Å, respectively, whereas the C5−N1 and C6−N2 distances are increased by 0.020 and 0.017 Å, respectively.

The glyoximes in **1** have an *E* configuration with O4−N2−C6−C5 torsion angle of $-179.82(18)^\circ$. The intramolecular inter-ligand O···O separations in these compounds are similar, lying between 2.462(3) and 2.547(3) Å. Such short O···O separations are often associated with symmetrical O···H···O hydrogen bonds [27].

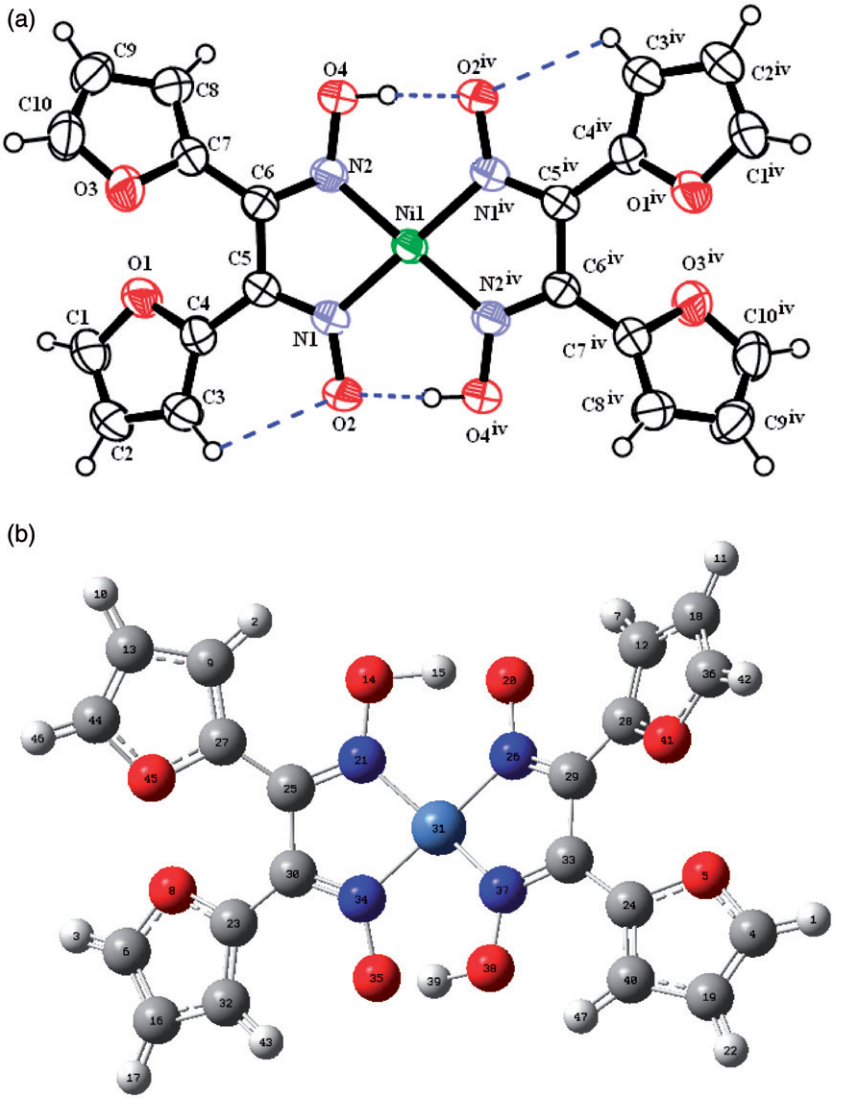

Figure 1. (a) ORTEP drawing of the basic crystallographic unit of **1** showing the atom-numbering scheme. Displacement ellipsoids are drawn at the 50% probability level and hydrogen atoms are shown as small spheres of arbitrary radii. Symmetry code: $^{iv}1-x, 1-y, 1-z$. (b) Gaussian 03 view drawing of **1**.

In **1**, one O-bound proton is lost from each ligand during complex formation and the remaining O-bound H participates in a very strong intramolecular hydrogen bond to the adjacent oxygen (table 3). The hydrogen was clearly visible in a difference map and, like the other complexes noted above, the O···H···O bond is not symmetrical. As can be seen from the packing diagrams (figure 2a and b), no classical intermolecular hydrogen-bonding is found but there are intramolecular hydrogen bonds such as an intra-ligand C–H···O and an inter-ligand O···H···O hydrogen bond in the crystal packing. Figure 2(a) shows Ni in the unit cell whereas figure 2(b) shows all the molecules. The packing diagram (figure 2a) has two different planes. Ni having (x, y, z)

Table 2. Selected geometrical parameters of **1** with X-ray structure and the DFT method.

	Experimental	B3LYP 3-21 G	B3LYP LANL2DZ
Ni1–N1	1.866(3)	1.812	1.899
Ni1–N2	1.873(2)	1.821	1.894
N1–O2	1.330(3)	1.390	1.355
N2–O4	1.339(3)	1.390	1.380
N1–C5	1.310(3)	1.322	1.332
N2–C6	1.299(3)	1.323	1.327
C5–C6	1.476(3)	1.474	1.491
C4–O1	1.361(3)	1.404	1.408
C7–O3	1.365(3)	1.405	1.407
C3–C4	1.351(4)	1.379	1.388
C7–C8	1.347(4)	1.379	1.388
N1–Ni1–N2	82.53(8)	83.22	82.62
O2–N1–Ni1	123.16(16)	122.03	122.07
O2–N1–C5	120.3(2)	118.70	121.39
O4–N2–Ni1	123.39(15)	124.40	122.94
O4–N2–C6	119.6(2)	117.44	119.91
C5–N1–Ni1	116.27(17)	117.52	116.11
C6–N2–Ni1	116.16(16)	116.70	115.77
C1–O1–C4	106.5(2)	106.52	106.93
C7–O3–C10	106.0(2)	106.54	106.95
C5–C4–O1	116.6(2)	118.97	117.78
C6–C7–O3	115.5(2)	118.52	117.57
O2–N1–Ni1–N2	173.91(17)	168.95	173.80
O4–N2–Ni1–N1	175.57(18)	171.49	172.94
Ni1–N1–C5–C4	172.40(17)	163.05	164.07
Ni1–N2–C6–C7	166.92(15)	161.38	163.87
O2–N1–C5–C6	−179.11(18)	−177.05	−179.60
O4–N2–C6–C5	−179.82(18)	−179.82	−179.69
N1–C5–C4–O1	−159.7(2)	−162.06	−153.97
N2–C6–C7–O3	−141.2(2)	−159.77	−154.28

Table 3. Hydrogen-bond interactions of **1** (Å, °).

Hydrogen bond (Å, °)	D–H	H···A	D···A	D–H···A
O4···H4···O2^{iv}	0.87(3)	1.58(2)	2.446(2)	173(5)
C3–H3···O2	0.93	2.46	2.855(3)	106

Symmetry code: $^{iv}1-x, 1-y, 1-z$.

and $(1/2-x, y, -z)$ symmetries locate in the same plane whereas Ni having $(1/2+x, 1/2-y, 1/2-z)$ symmetry code locates in the other plane. These nickels are centered in sites of the unit cell such as at $[1/2+n, 1/2+m, 1/2+k]$, $[n, 1/2+m, 1/2+k]$, and $[1/2+n, m, k]$, respectively ($n, m,$ and k are zero or integer), and these planes are running along the *c*-axis of the orthorhombic cell.

3.2. *Theoretical structures*

The optimized molecular structure is shown in figure 1(b). Some selected geometric parameters experimentally obtained and theoretically calculated by B3LYP/3-21 G and

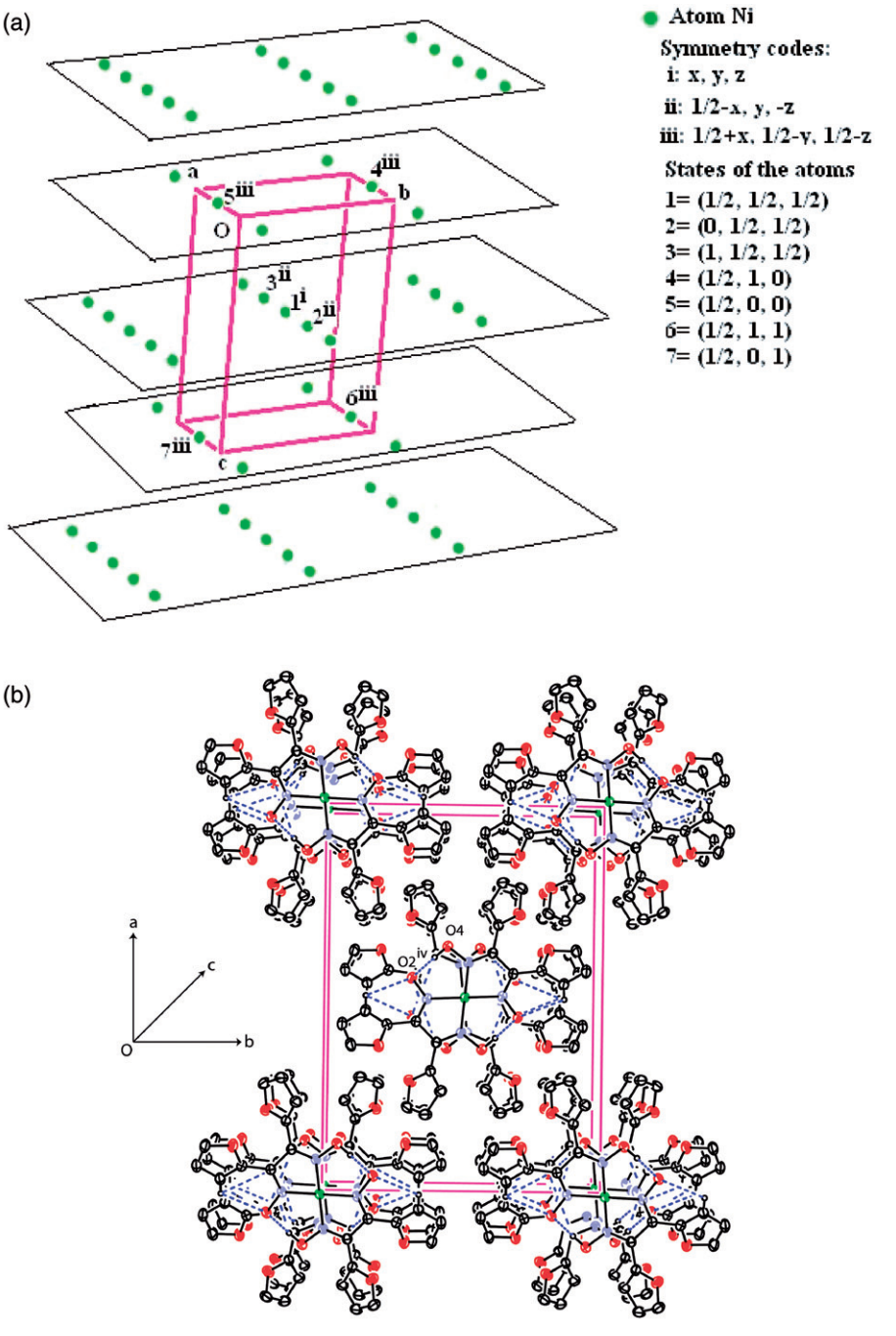

Figure 2. (a) A partial packing diagram of **1**. Hydrogen atoms and other atoms except Ni have been omitted. (b) A partial packing diagram of **1**. Hydrogen atoms have been omitted. Symmetry code: $^{iv}1-x$, $1-y$, $1-z$.

Table 4. Vibrational frequencies of **1** with experimental and DFT/B3LYP methods.

Frequencies	Experimental	B3LYP 3-21 G	B3LYP LANL2DZ
ν(OH)	3801–3425	1375–1266/1001	1616/1593/1445
ν_s(CH)	3145	3362–3359	3337
ν_{as}(CH)	3125	3326–3292	3329–3290
δ(O···H···O)	1748	1853–1848	1863–1854
ν(C=C)	1519	1601–1588	1623/1522
ν(C=N) + δ(OH)	1580	1533–1538	1863/1614/1556
ρ_t(CH) + ν(CO)	1479	1243	1241
ν(CC) + ν(O···H···O)	1375	1375–1266	1445/1342
ν(CC) + δ(OH)	1375	1241	1342–1306
ν(NO) + δ(CH)	1290	1336–1306/1174	1306/1194/1102
ν(CN) + ν(CC) + δ(OH)	1243	1483	1499
ρ_t(OH)	1221	1135	1133
ρ_t(CH)	1151	1079	1084
ν(CO) + ρ_t(CH)	1133	1079–1076	1080/1040
ρ_s(CH)	1084	1076–1053	1169
ν(NO) + ν(O···H···O)	1015	1001	1064/1032
ρ_t(COC)	865	905/874	950
t(CH)	814	939	935
w(CH)	762–734	883/766	879/773
δ(CH) out of plane	734	715	680

ρ_t: rocking, t: twist, δ: bending, ρ_s: scissoring, ν_s: symmetric stretching, ν_{as}: asymmetric stretching, w: wagging.

B3LYP/LANL2DZ methods are listed in table 2. The optimized molecular geometry is shown in figure 1(b) with dihedral angles between A, B, and C planes calculated at 18.51° (A/C), 38.85° (B/C), and 45.69° (A/B) for B3LYP/LANL2DZ and 18.51° (A/C), 38.84° (B/C), and 45.70° (A/B) for B3LYP/3-21 G. Experimental results are solid phase and theoretical calculations are gaseous phase. In the solid state, intermolecular interactions connect molecules, resulting in differences of bond parameters between calculated and experimental values. DFT optimized geometric parameters are usually in good agreement with experimental values and more accurate than Hartree–Fock and semi-empirical methods, due to inclusion of electron correlation. The largest differences between experimental and calculated bond lengths, bond angles, and torsion angles are 0.060 Å and 0.047 Å, 3.02° and 2.07°, 5.54° and 13.03° for B3LYP/3-21 G and B3LYP/LANL2DZ, respectively. Optimized bond lengths and angles provided by B3LYP/LANL2DZ are the closest to the experimental values (see table 2) whereas the torsion angles provided by B3LYP/3-21 G show the best agreement with the experimental values.

3.3. *Vibrational frequency*

Vibrational frequencies are calculated at the B3LYP/3-21 G and B3LYP/LANL2DZ levels for **1**. Some primary calculated harmonic frequencies are listed in table 4 and compared with experimental data; assignments are also indicated in table 4. Gaussview molecular visualization program was used to assign the calculated harmonic frequencies. IR spectra of **1** has been studied to characterize its structure; experimental FT-IR spectra are provided in "Supplementary material." *Ab initio* calculations systematically overestimate the vibrational wavenumbers and discrepancies. Generally, oximes are

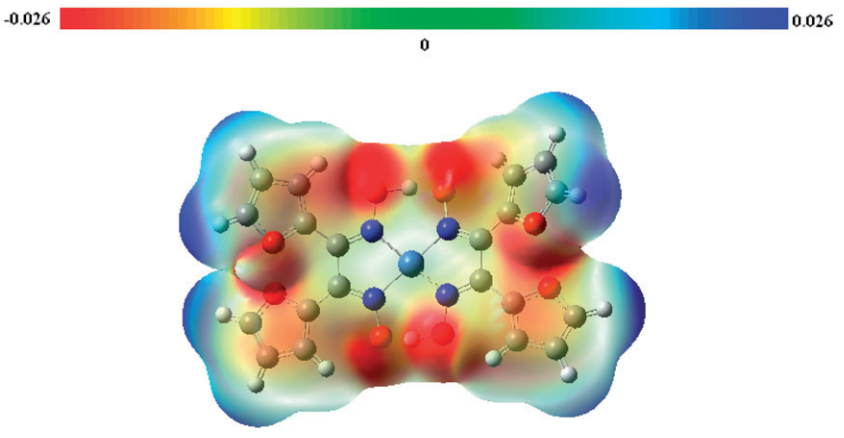

Figure 3. MEP map (in a.u.) of **1** with the B3LYP/3-21 G method (with an isodensity value of 0.0004 a.u.).

characterized by three IR absorptions at 3300–3150 cm^{-1} (O–H str.), 1690–1620 cm^{-1} (C=N str.), and 950 cm^{-1} (N–O str.) [7].

As shown in table 4, experimentally determined vibrational bands were significantly lower than calculated values, however, ν(OH) stretching vibrations are at 3801–3425, 1375–1266/1001, and 1616/1593/1445 cm^{-1} and one of the bending vibrations at 1243, 1483, and 1493 cm^{-1} for experimental and theoretical (B3LYP/3-21 G and LANL2DZ) values, respectively. Due to O···H···O hydrogen-bonding, experimental δ(OH) bending vibration increases while ν(OH) stretching vibration decreases [28].

In the literature, the free *vic*-dioxime ligand shows a strong peak at 1638 cm^{-1} for LH_2, which is characteristic of the azomethine ν(C=N) group [29]. Coordination of the *vic*-dioxime ligands to the metal center through the four nitrogen atoms are expected to reduce the electron density in the azomethine link and lower the ν(C=N) absorption frequency. As can be seen from table 4 and figure 3, the peak due to ν(C=N) is shifted to lower frequencies and appears at 1580 cm^{-1}, indicating coordination of the azomethine nitrogen to the nickel metal [30]. This ν(C=N) vibration mode is calculated with the B3LYP/3-21 G and the B3LYP/LANL2DZ methods at 1533–1538 cm^{-1}, and 1556 cm^{-1}, respectively. However, the disappearance of ν(O–H) stretching bands in the IR spectrum of free ligand together with the existence of H-bridge (O···H···O) at 1748 cm^{-1} and the shifting of −C=N and −N–O stretches in the IR spectra of the metal complex (1) provide support for MN_4-type coordinations in the metal complexes [31]. The characteristic δ(O···H···O) bending vibration of the optimized molecule is calculated at 1853–1848 cm^{-1} for the B3LYP/3-21 G and 1863–1854 cm^{-1} for the B3LYP/LANL2DZ methods. These values are in accord with previously reported oxime derivatives [7, 9, 32–34]. The other calculated vibrational frequencies can be seen in table 4. In general, when the calculated IR frequencies are compared with the experimental data of **1**, all data agree with calculated vibrations.

3.4. *Assignments of the chemical shift values*

DFT methods treat the electronic energy as a function of the electron density of all electrons simultaneously and thus include electron correlation effect. We explicitly

Table 5. Theoretical and experimental ^{13}C and ^{1}H isotropic chemical shifts (with respect to TMS all values in ppm) for **1**.

Atoms	Experimental	B3LYP/3-21 G	B3LYP/LANL2DZ
C4	118.170	133.811	150.616
C6	118.170	133.591	150.462
C9	117.62	112.789	128.099
C12	117.62	113.208	128.591
C13	112.46	102.428	113.236
C16	112.46	102.428	113.236
C18	112.46	102.185	112.690
C19	112.46	102.428	113.050
C23	144.50	136.424	152.654
C24	144.50	136.480	152.399
C25	159.50	135.777	150.690
C27	144.50	136.587	152.654
C28	144.50	136.281	152.196
C29	159.50	135.192	150.077
C30	159.50	136.689	152.196
C32	117.62	112.638	127.94
C33	159.50	136.480	150.690
C36	118.170	133.698	150.363
C40	117.62	113.306	128.876
C44	118.170	133.811	150.553
H1	7.370	7.338	7.963
H2	7.690	8.251	8.850
H3	7.370	7.338	7.963
H7	7.690	8.349	8.913
H10	6.845	6.283	6.915
H11	6.845	6.283	6.915
H15	12.206	19.397	18.746
H17	6.845	6.283	6.915
H22	6.845	6.283	6.915
H39	12.206	19.680	19.049
H42	7.370	7.338	7.963
H43	7.690	8.349	8.913
H46	7.370	7.338	7.963
H47	7.690	8.251	8.913

considered the influence of the level used for the geometry optimization on the final value of **1** when GIAO ^{13}C and ^{1}H c.s. calculations were obtained at the B3LYP/3-21 G and B3LYP/LANL2DZ levels of theory for the two optimized geometries. The results of these calculations are tabulated in table 5. The theoretical ^{13}C and ^{1}H chemical shift values (with respect to TMS) of **1** are generally compared to the experimental ^{13}C and ^{1}H chemical shift values. These results are also shown in table 5. The ^{1}H chemical shift values (with respect to TMS) have been calculated to be 19.680–6.283 ppm with the B3LYP/3-21 G level and 19.049–6.915 ppm with the B3LYP/LANL2DZ level. The ^{1}H-NMR spectrum of the nickel(II) complex shows 12.206 ppm supporting the proposed (O−H $\cdots$ O) bridge, and this result can be easily identified by deuterium exchange. This has been calculated at 19.397, 19.680 ppm and 18.746, 19.049 ppm using the B3LYP/3-21 G and the B3LYP/LANL2DZ levels for H15 and H39 atoms bound to oxime, respectively. In the ^{13}C-NMR the carbon resonances of the oximes appear at 159.50 ppm and are found to be 135.777, 135.192, 136.689, and 136.480 ppm by the B3LYP/3-21 G and 150.690, 150.077, 152.196, and 150.690 ppm by the B3LYP/LANL2DZ levels.

Table 6. MO energies of **1** with the DFT method.

Energies	B3LYP/3-21 G	B3LYP/LANL2DZ
HOMO (a.u.)	−0.197	−0.215
LUMO (a.u.)	−0.104	−0.109
Δ (a.u.) (eV)	0.093 (2.530)	0.106 (2.884)
Total energies (a.u.)	−3083.513	−1760.234
Dipole moment (Debye)	1.093	0.0004
HOMO −1 (a.u.)	−0.206	−0.217
HOMO −2 (a.u.)	−0.215	−0.232
LUMO +1 (a.u.)	−0.072	0.091
LUMO +2 (a.u.)	−0.039	0.069

1 a.u. = 27.2116 eV.

3.5. *Molecular electrostatic potential*

MEP is related to electron density and is a very useful descriptor in understanding sites for electrophilic attack and nucleophilic reactions as well as hydrogen-bonding interactions [35]. To predict reactive sites for electrophilic attack for **1**, MEP was calculated at the B3LYP/3-21 G optimized geometry. The negative regions of MEP were related to electrophilic reactivity and the positive ones to nucleophilic reactivity (shown in figure 3). As can be easily seen in figure 3, this molecule has three possible sites for electrophilic attack. The negative regions are mainly over oxygen atoms with O2 more negative than O1, O2, and O3 atoms.

3.6. *FMO analysis*

The calculations indicate that **1** has 127 occupied molecular orbitals (MOs). The HOMO energies, the LUMO energies, and the energy gaps are given in table 6. The frontier MOs play an important role in electrical and optical properties, as well as in UV-Vis spectra and chemical reactions [36]. Based on the B3LYP/3-21 G and B3LYP/LANL2DZ optimized geometries, the total energy of **1** has been calculated by these methods, as −3083.513 and −1760.234 a.u., respectively. An electronic system with a larger HOMO–LUMO gap should be less reactive than one having a smaller gap [37]. In this study, the HOMO–LUMO gaps of the molecule are at 2.530 and 2.884 eV for the B3LYP/3-21 G and B3LYP/LANL2DZ methods, respectively (table 6), and this energy gap indicates that the structure is very stable.

UV-Vis absorption spectra of **1** were recorded in DMSO. The 232, 271, 285, and 435 nm bands are due to three $\pi \rightarrow \pi^*$ transitions of C=N and a charge-transfer transition arising from π electron interactions between the metal and ligand involving either a metal-to-ligand or ligand-to-metal electron transfer [38]. Unfortunately, the $n \rightarrow \pi^*$ transition was obscured by the $\pi \rightarrow \pi^*$ transitions and the weak d−d transitions were not observed. The calculated electron transfers (ET) with B3LYP/3-21 G and B3LYP/LANL2DZ are at 259, 273, 289, and 451 nm and 280, 308, 313, and 423 nm to correspond to the UV-Vis spectral absorptions, and the corresponding ET between HOMO −2 → LUMO +2, HOMO −1 → LUMO +2, HOMO → LUMO +2, and HOMO −1 → LUMO, respectively. 3-D plots of HOMO −2, HOMO −1, HOMO, LUMO, LUMO +1, LUMO +2 and the corresponding energy levels for **1** are shown in figure 4.

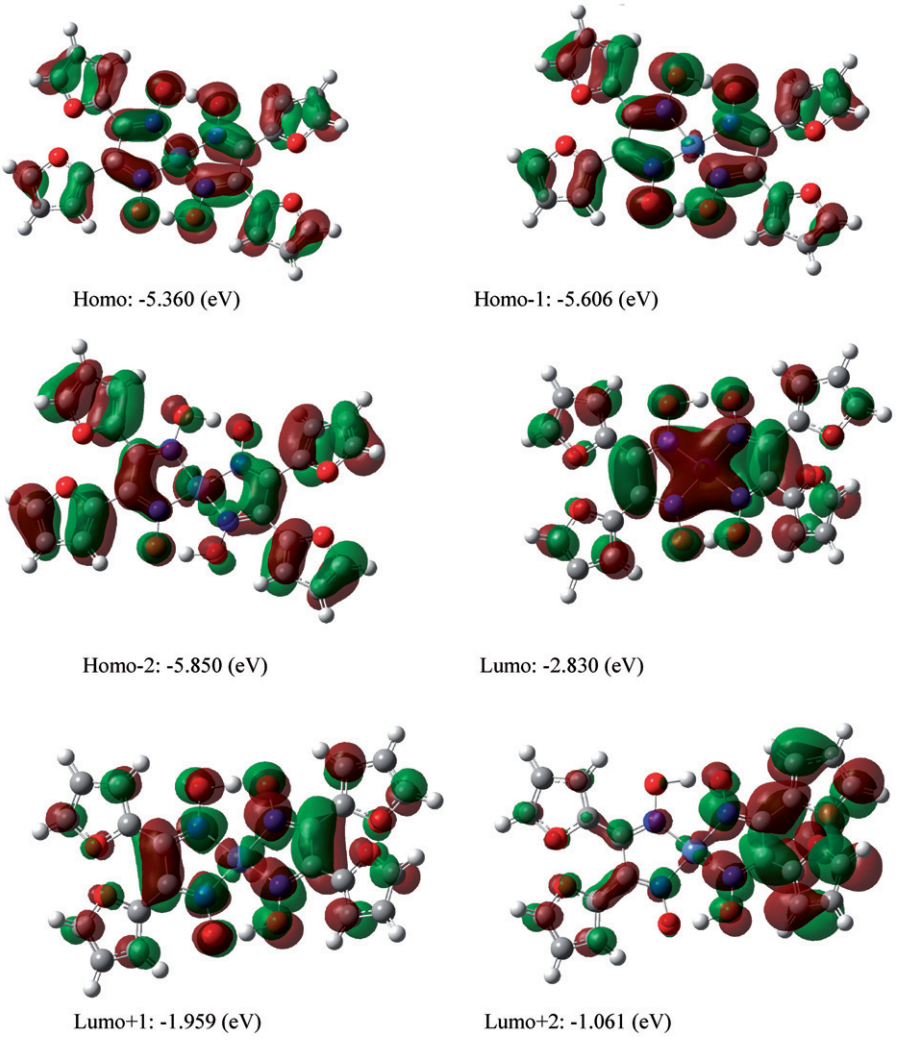

Figure 4. MO surfaces and energy levels given in parentheses for the HOMO −2, HOMO −1, HOMO, LUMO, LUMO +1, and LUMO +2 of **1** computed with the B3LYP/3-21 G method.

3.7. *Magnetic studies*

The magnetic susceptibility measurement of **1** indicates diamagnetism.

Supplementary material

Crystallographic data for the structural analysis have been deposited with the Cambridge Crystallographic Data Centre, CCDC No. 806162. Copies of this

information may be obtained free of charge from the Director, CCDC, 12 Union Road, Cambridge CB2 1EZ, UK (Fax: +44-1223-336033; E-mail: deposit@ccdc.cam.ac.uk or www: http://www.ccdc.cam.ac.uk).

Acknowledgments

The authors acknowledge the Faculty of Arts and Sciences, Ondokuz Mayis University, Turkey, for the use of the STOE IPDS-II diffractometer (purchased under grant F.279 of the University Research Fund).

References

[1] E. Canpolat, A. Yazıcı, M. Kaya. *Trans. Met. Chem.*, **31**, 653 (2006).
[2] A. Coşkun, İ. Karataş. *Turk. J. Chem.*, **28**, 173 (2004).
[3] K. Yabuuchi, D. Kawamura, M. Inokuchi. *Mol. Cryst. Liq. Cryst.*, **455**, 81 (2006).
[4] A. Yılmaz, B. Taner, P. Deveci, A.Y. Obalı, U. Arslan, E. Şahin, H.İ. Uçan, E. Özcan. *Polyhedron*, **29**, 2991 (2010).
[5] A. Kılıç, A. Tas, I. Yılmaz. *J. Chem. Sci.*, **121**, 43 (2009).
[6] H. Batı, A. Zulfikaroglu, M. Tas, O. Andac, W.T.A. Harrison. *Acta Cryst.*, **E61**, m2033 (2005).
[7] H. Batı, A. Zulfikaroglu, M. Tas, N. Çalışkan, S. Soylu, O. Andac, O. Büyükgüngör. *Acta Cryst.*, **E60**, m1334 (2004).
[8] S. Serin, S.B. Oksal, O. Serindag. *Synth. React. Inorg. Met.-Org. Chem.*, **22**, 195 (1992).
[9] E. Canpolat, M. Kaya. *J. Coord. Chem.*, **55**, 1419 (2002).
[10] P. Chaudhuri. *Coord. Chem. Rev.*, **243**, 143 (2003).
[11] A. Chakravorty. *Coord. Chem. Rev.*, **1**, 1 (1974).
[12] A. Kakanejadifard, E. Niknam, A. Zabardasti. *J. Coord. Chem.*, **60**, 677 (2007).
[13] K.T. Das, B.K. Bera, A.K. Datta, A.K. Ghosh. *Trans. Met. Chem.*, **34**, 247 (2009).
[14] Stoe&Cie. *X-AREA (Version 1.18) and X-RED32 (Version 1.04)*, Stoe&Cie, Darmstadt, Germany (2002).
[15] G.M. Sheldrick. *SHELXS-97 and SHELXL-97*, University of Göttingen, Germany (1997).
[16] L.J. Farrugia. *ORTEP-3*, University of Glasgow, UK (1998).
[17] A.D. Becke. *J. Chem. Phys.*, **98**, 5648 (1993).
[18] C. Lee, W. Yang, R.G. Parr. *Phys. Rev.*, **B37**, 785 (1988).
[19] R. Ditchfield. *J. Chem. Phys.*, **56**, 5688 (1972).
[20] K. Wolinski, J.F. Hinton, P. Pulay. *J. Am. Chem. Soc.*, **112**, 8251 (1990).
[21] A. Frish, A.B. Nielseni, A.J. Holder. *Gaussview User Manual,* Gaussian Inc., Pittsburgh, PA (2001).
[22] M.J. Frisch, G.W. Trucks, H.B. Schlegel, G.E. Scuseria, M.A. Robb, J.R. Cheeseman, J.A. Montgomery, T. Vreven, K.N. Kudin, J.C. Burant, J.M. Millam, S.S. Iyengar, J. Tomasi, V. Barone, B. Mennucci, M. Cossi, G. Scalmani, N. Rega, G.A. Petersson, H. Nakatsuji, M. Hada, M. Ehara, K. Toyota, R. Fukuda, J. Hasegawa, M. Ishida, T. Nakajima, Y. Honda, O. Kitao, H. Nakai, M. Klene, X. Li, J.E. Knox, H.P. Hratchian, J.B. Cross, C. Adamo, J. Jaramillo, R. Gomperts, R.E. Stratmann, O. Yazyev, A.J. Austin, R. Cammi, C. Pomelli, J.W. Ochterski, P.Y. Ayala, K. Morokuma, G.A. Voth, P. Salvador, J.J. Dannenberg, V.G. Zakrzewski, S. Dapprich, A.D. Daniels, M.C. Strain, O. Farkas, D.K. Malick, A.D. Rabuck, K. Raghavachari, J.B. Foresman, J.V. Ortiz, Q. Cui, A.G. Baboul, S. Clifford, J. Cioslowski, B.B. Stefanov, G. Liu, A. Liashenko, P. Piskorz, I. Komaromi, R. Martin, D.J. Fox, T. Keith, M.A. Al-Laham, C.Y. Peng, A. Nanayakkara, M. Challacombe, P.M.W. Gill, B. Johnson, W. Chen, M.W. Wong, C. Gonzalez, J.A. Pople. *Gaussian 03*, Gaussian, Inc., Wallingford, CT (2004).
[23] A.W. Marsman, E.D. Leussink, J.W. Zwikker, L.W. Jenneskens. *Chem. Mater.*, **11**, 1484 (1999).
[24] V. Bertolasi, G. Gilli, A.C. Veronese. *Acta Cryst.*, **B38**, 502 (1982).
[25] L. Chertanova, C. Pascard, A. Sheremetev. *Acta Cryst.*, **B50**, 708 (1994).
[26] T. Hökelek, A. Zülfikaroğlu, H. Batı. *Acta Cryst.*, **E57**, o1247 (2001).
[27] A. Chakravorty. *Coord. Chem. Rev.*, **13**, 1 (1974).
[28] R.M. Silverstein, G.C. Bassler, T.C. Morrill. *Spectrometric Identification of Organic Compounds*, Wiley & Sons, New York (1963).

[29] (a) K.N. Kumar, R. Ramesh. *Polyhedron,* **24**, 1885 (2005); (b) A. Kilic, E. Tas, B. Gumgum, I. Yılmaz. *Trans. Met. Chem.,* **31**, 645 (2006).
[30] S.A. Ali, A.A. Soliman, M.M. Aboaly, R.M. Ramadan. *J. Coord. Chem.*, **55**, 1161 (2002).
[31] (a) M. Kandaz, A. Koca, A.R. Ozkaya. *Polyhedron,* **23**, 1987 (2004); (b) E. Tas, M. Aslanoglu, A. Kilic, Z. Kara. *J. Coord. Chem.,* **59**, 861 (2006).
[32] M. Macit, H. Batı, B. Batı. *Turk. J. Chem.*, **24**, 81 (2000).
[33] E. Özcan, E. Karapınar, N. Karapınar. *Synth. React. Inorg. Met.-Org. Chem.*, **31**, 1163 (2001).
[34] R. Güp, H.K. Alpgüz, A.D. Bedük. *Collect. Czech. Chem. Commun.*, **67**, 209 (2002).
[35] Ç. Yüksektepe, H. Saraçoğlu, N. Çalışkan, I. Yılmaz, A. Cukurovali. *Bull. Korean Chem. Soc.*, **31**, 3553 (2010).
[36] I. Fleming. *Frontier Orbitals and Organic Chemical Reactions*, Wiley, London (1976).
[37] R. Kurtaran, S. Odabaşoğlu, A. Azizoğlu, H. Kara, O. Atakol. *Polyhedron*, **26**, 5069 (2007).
[38] E. Tas, M. Ulusoy, M. Guler, I. Yılmaz. *Trans. Met. Chem.*, **29**, 180 (2004).